Research Article Vol. 30, No. 23 / 7 Nov 2022 / Optics Express 41399
Optics EXPRESS

Plasmonic nanolaser based on a single oligomer

IGOR A LITVIN[1,*] AND STEPHANIE REICH[1,2]

[1] Institut für Experimental Physik, Freie Universität Berlin, 14195 Berlin, Germany
[2] reich@physik.fu-berlin.de
[*] ilitvin@physik.fu-berlin.de

Abstract: We investigate the effect of manipulating the laser quality factor and the spectral properties of the gain medium on an oligomer-based plasmonic nanolaser. We develop different designs of the oligomer resonators, decreasing the lasing threshold and increasing the mode lifetime to improve the lasing efficiency. Based on the designs we are able to decrease the lasing threshold by a factor of ten. We discuss and show numerically the influence of the oligomer geometry, the lasing mode oscillation lifetime, and the photoluminescence peak linewidth of the gain medium on the lasing efficiency of the oligomer based plasmonic nanolaser.

1. Introduction

The localised surface plasmons (LSP) of metallic nanostructures have been intensively investigated due to their unique potential to manipulate light at the nanometer scale [1,2]. The LSP of metallic nanostructures are able to confine electromagnetic energy beyond the diffraction limit [2]. The surface plasmons (SPs) also produce strong, localised electromagnetic fields (hot spots) that enhance optical processes by many orders of magnitude [3]. Based on their lifetime and dipole moment, plasmonic modes are divided into bright and dark [4,5]. Bright modes have a net dipole moment. They are excited by far-field radiation (linear- or unpolarized light) and decay as reemitted photons on a time scale of ~5 fs. The net dipole moment of dark plasmons vanishes. They have longer lifetimes (~20 fs) because the emission of photons into the far field is strongly reduced [6,7]. The selective excitation of a given eigenmode in a plasmonic oligomer would be a powerful tool to manipulate the plasmon oscillation time, absorption and scattering, hot spot position, frequency, and far-field electromagnetic radiation.

The unique properties of the LSP can be utilised to design lasers with nanoscale dimensions [8,9]. A number of plasmonic nanolasers were reported recently based on different nanocavity designs and gain media: lasers using a hybrid plasmonic waveguide consisted of a high-gain cadmium sulphide semiconductor nanowire, separated from a silver surface by a 5-nm-thick insulating gap [10]; plasmonic nanoarray laser based on split-ring resonators with curved plasmonic nanowire pair subunits of different lengths [11]; a single mode lasing from an arrays of plasmonic nanocavities in a homogeneous dielectric environment at room temperature [12]; tunable lattice plasmon lasing from an arrays of gold nanoparticles and liquid gain materials [13]; a dark plasmonic mode laser based on an array of metallic nanorods in an optically pumped organic dye gain medium [14]; a Nd^{3+} solid-state laser based on chains of metallic nanoparticles [15]; a monolithically fabricated ZnO/Al plasmonic-waveguide nanolaser [16] and so on.

The properties of LSP can be applied to manipulate the quality factor of the nanolaser resonator, increasing the lasing efficiency and decreasing the lasing threshold. Namely, the emitting wavelength of such a nanolaser can be adjusted to the energy region of low bulk metal absorption and a long lifetime mode can be chosen to increase the lasing efficiency. Moreover, the hot spots create regions with higher pump intensity decreasing the lasing threshold [17]. Implementing nano oligomers as a laser resonator decreases the size of the nanolaser (in comparison to nano array nanolaser) and can potentially minimise many optical devices such as biosensors, solar cells, and photodetectors [18,19]. Furthermore, plasmonic nanolasers also offer the ability to

#472812 https://doi.org/10.1364/OE.472812
Journal © 2022 Received 9 Aug 2022; revised 20 Sep 2022; accepted 21 Sep 2022; published 26 Oct 2022

Optics EXPRESS

amplify weak physical and chemical light-matter interactions due to the tightly focused, enhanced optical fields supported by SPs. Additionally, the oscillation of a particular lasing mode supports a stimulated emission by a plasmonic nanolaser and can be used for the selective excitation of specific LSP [20].

Conventional gain materials that can compensate for losses in plasmonic nanolasers are inorganic semiconductors [21,10] and organic dye molecules [21]. Semiconductors exhibit high non-radiative recombination rates, which reduces the optical gain at room temperature. The room-temperature lasing operation could be achieved in nanowire-on-film systems by designing the nanocavities to suppress radiative losses [10]. On the other side, organic dye molecules have high quantum yields and can readily compensate metal loss and achieve lasing at room temperature [21]. They can be incorporated in silica shells or in a polymer matrix surrounding the plasmonic nanoparticles (NPs); however, a disadvantage is the photo-induced bleaching of their fluorescence that can decrease their long-term stability under high pump intensities.

In this work we study the influence of the laser quality factor in the nano oligomer based nanolaser. We consider various oligomer designs (2-18 gold nano discs) for the laser resonator, which result in different lifetime of the lasing mode, to improve the lasing efficiency and decrease the lasing threshold. We have shown that increasing the number of discs (geometry complexity) of a nano oligomer affects the plasmon lifetime and raises the lasing efficiency. Due to the presence of areas of increased electric field intensity (the hot spots) in the nano-oligomers, the lasing threshold decreases as well. The spatial property of the output beams for such nanolasers depends on the particular oligomer geometry and can be tailored. This opens a wide range of possibilities for both laser beam shaping and laser beam engineering, to manipulate the spatial and temporal properties of the output beam.

2. Method

We simulated the localised plasmon excitation and respective oligomer response with the finite-difference time-domain (FDTD) method [22], using the commercial software package Lumerical FDTD Solutions. The simulations were performed with the experimentally obtained Johnson–Christy dielectric function of gold [22]. The incident Gaussian beam was simulated with its amplitude, polarisation and spatial properties by an embedded scripting language in the FDTD software. Additionally, we have used the boundary elements method [23] to obtain the charge density image of the oligomer eigenmodes and their eigenvalues. This approach helped to develop an oligomer design that provides an lasing mode oscillating at the photoluminescence (PL) maximum of a given gain material.

We simulated the lasing dynamics with the FDTD computational model of a four-level two-electron atomic system. Transitions between the energy levels are governed by coupled rate equations and the Pauli Exclusion Principle [24]. In the model, the gain medium (IR-140 organic dye and Nd^{3+}:YAG) is a four-level quantum system (see Fig. 1), the electromagnetic field is modelled by classical electrodynamics [24]. An incident pump pulse excites the electron population density from level 0 to level 3. The population density of the excited levels 3 and 1 decay fast and non-radiatively to level 2 and 0 respectively. In the case of the population inversion between levels 2 and 1 we reach lasing emission. In the model all radiative transitions (21, 03, see Fig. 1) can be considered as two coupled dipole oscillators. Levels 0 and 3 are coupled by dipole P_{30} and levels 1 and 2 are coupled by dipole P_{21}; γ_{30} and γ_{21} are dephasing rates of dipole P_{30} and dipole P_{21} respectively [24]. The equations that govern the dynamics of polarization densities are given by:

$$\frac{\partial^2 P_a}{dt^2} + \gamma_0 \frac{dP_a}{dt} + \omega_a^2 P_a = \vartheta_a (N_2 - N_1) E, \tag{1a}$$

Optics EXPRESS

$$\frac{\partial^2 P_b}{dt^2} + \gamma_0 \frac{dP_b}{dt} + \omega_b^2 P_b = \vartheta_b (N_3 - N_0) E, \tag{1b}$$

where $\vartheta_{a,b} = 6\pi\varepsilon c^3/(\omega_{21,30}^2 \tau_{21,30})$, $\boldsymbol{Pa}$ and $\boldsymbol{Pb}$ have the resonant frequencies ω_a and ω_b; $\hbar\omega_a$ is the energy difference between levels 1 and 2 and $\hbar\omega_b$ is the energy difference between levels 0 and 3.

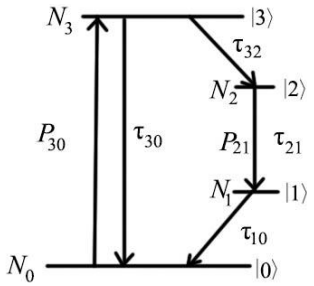

Fig. 1. Four-level two-electron model [25].

The population densities of the various levels of the gain medium are given by the coupled rate equations [24]:

$$\frac{dN_3}{dt} = -\frac{N_3(1-N_2)}{\tau_{32}} - \frac{N_3(1-N_0)}{\tau_{30}} + \frac{1}{h\omega_b} E \frac{dP_b}{dt}, \tag{2a}$$

$$\frac{dN_2}{dt} = -\frac{N_3(1-N_2)}{\tau_{32}} - \frac{N_2(1-N_1)}{\tau_{21}} + \frac{1}{h\omega_a} E \frac{dP_a}{dt}, \tag{2b}$$

$$\frac{dN_1}{dt} = -\frac{N_2(1-N_1)}{\tau_{21}} - \frac{N_1(1-N_0)}{\tau_{10}} - \frac{1}{h\omega_a} E \frac{dP_a}{dt}, \tag{2c}$$

$$\frac{dN_0}{dt} = -\frac{N_3(1-N_0)}{\tau_{30}} - \frac{N_1(1-N_0)}{\tau_{10}} - \frac{1}{h\omega_b} E \frac{dP_b}{dt}. \tag{2d}$$

Equations (1) and (2) are coupled to Maxwell-Ampere's law given by [25]:

$$\frac{dE}{dt} = \frac{1}{\varepsilon}\left(\nabla \times H - N_d \left(\frac{dP_a}{dt} + \frac{dP_b}{dt}\right)\right), \tag{3}$$

where ε is the material permittivity, **E** and **H** are the electric and magnetic fields respectively. Equations (1)–(3) provide us with a set of self-consistent equations, which are numerically solved to calculate the time-resolved dynamics of the gain medium in response to optical pumping.

Based on the approach described in the Eq. (1)–(3), we simulated the lasing dynamic of the plasmonic nanolasers using the full-field vectorial electromagnetic simulator implemented in Lumerical FDTD Solutions.

To reach efficient lasing, the electric field distribution must spatially fit the selected pump mode. The pump efficiency can be obtained from the maximum value of a fitting integral P_i that describes the coupling of the pump mode to the lasing mode [25,26]:

$$P_i = \frac{\iiint_V dr^3 \vec{M}_i(\vec{r}) \vec{E}_0(\vec{r})}{\iiint_V dr^3 |\vec{E}_0(\vec{r})|^2}, \tag{4}$$

where $\vec{M}_i(\vec{r})$ is the electric field of the lasing eigenmode i, $\vec{E}_0(\vec{r})$ is the electric field of the pumping mode. The integral must be taken over the gain volume V (outside the oligomer).

Optics EXPRESS

Additionally, the spontaneous emission rate of an emitter is proportional to the local density of optical states (LDOS) and can be enhanced in a cavity by the Purcell factor $F \sim (Q/V_m)(\lambda/n)^3$ in accordance with Fermi's golden rule [27,28]; where V_m - the mode volume, Q - the cavity quality factor, λ - the resonant wavelength and n - the refractive index. Increasing the LDOS simultaneously increases the rate of spontaneous and stimulated emission processes during lasing and improves the laser efficiency [29]. The mode volumes V_m of the plasmonic nanolasers cavities are ultrasmall and can increase the LDOS up to 10^4 times. To increase the Purcell factor and LDOS, the quality factor of the plasmonic nanolaser (which is proportional to . . . [30]) must be maximised.

3. Oligomer modes

In this section we calculate the spectral and temporal properties of different oligomer geometries without gain medium to understand the behaviour of the nanolaser cavities and oscillating surface plasmons using the commercial software package Lumerical FDTD Solutions. We constructed a dimer, quadrumer, hexamer, decamer and 18-mer of gold nanodiscs (diameter $d = 100$ nm, gap size $a = 20$ nm, height $h = 30$ nm) (see Fig. 2(a)). The dimensions of the structures were chosen such that the size of the individual nanodisks is much smaller than the wavelength of the incident light, but the overall dimension of the oligomer is a considerable fraction of the beam width ($w_0 = 1$ μm). In our analysis, we will focus on oligomer modes with energies <2 eV (> 620 nm) because the modes with higher eigenenergies are damped by the interband transitions [31]. We observe the oscillating modes around 880 nm, which corresponds to the PL maximum of IR-140 organic dye to increase the future lasing efficiency.

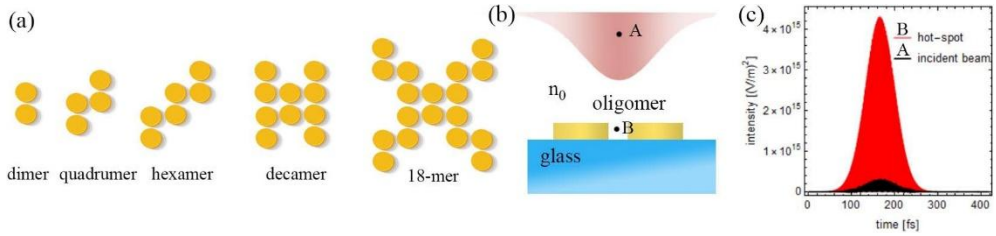

Fig. 2. (a) Geometry of the gold nanodisk oligomers (dimer, quadrumer, hexamer, decamer, 18-mer) considered in this work. (b) Schematic of the excitation of plasmonic modes in a gold oligomer on a glass plate. (c) The comparison of the intensity oscillation in the middle of the incoming Gaussian beam (A) and in the hot spot (B).

We investigated five different oligomer designs based on the gold nanodisc dimer as a basic design component (see Fig. 1(a)). The refractive index of the surrounded space was selected to fit the refractive index of the chosen gain material (IR-140 ($n_0 = 1.55$)). The gold oligomers were placed on top of a glass plate. The oligomer diameters and gaps between the oligomers were chosen to fit current parameters and limitations of Ga ion beam miing to produce the oligomer from the gold flakes (around 20 nm) [32]. We see ten-fold increase of the intensity in the hot spots (point B of Fig. 2(b)) in comparison to the incoming beam intensity at the maximum amplitude point (point A of Fig. 2(b)), for the particular case of the oligomer discs and gap sizes (see Fig. 2(c)). However, He ion beam milling provides gap sizes down to 3-5 nm that can increase the hot spot intensity and decrease the lasing threshold respectively [32].

Based on the simulation, we see that the lifetime of the plasmon oscillations increases by a factor of three from quadrumer to decamer (see Fig. 3(d-f)). This behaviour can be explained by spectral intersections (mismatches) and the resulting constructive (destructive) interference of plasmon resonances of the coupling parts of the complex oligomer. The result of this lifetime increase is a spectral linewidth decrease of the oligomer absorption spectra (see Fig. 3(a)) as

Optics EXPRESS

well as Fourier transform spectra of electric vector oscillation in the hot spot (see Fig. 3(b)). It means that we can expect the respective nanolaser resonator quality factor to increase (~6(dimer), ~8(quadrumer), ~19(decamer)) [30] and, as a result, the growth of the lasing efficiency.

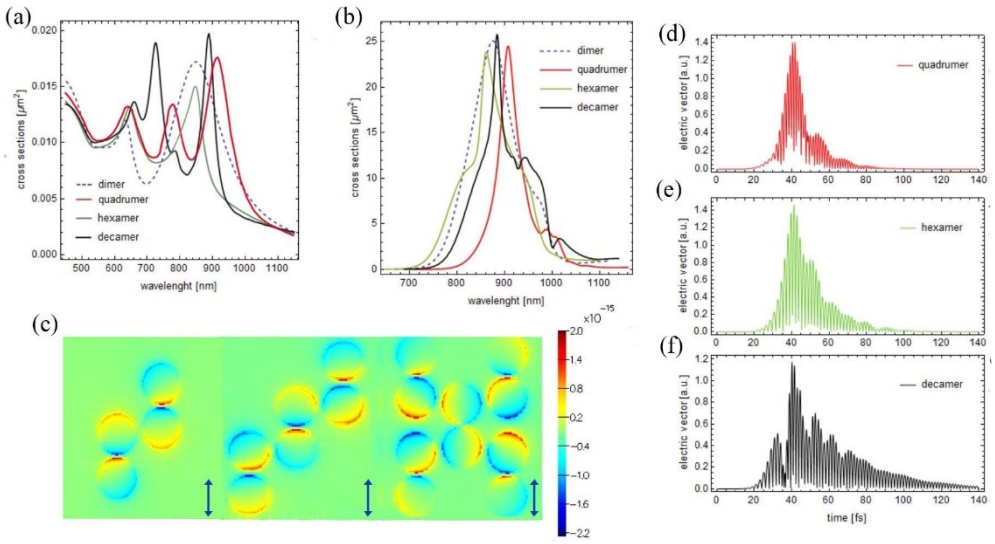

Fig. 3. (a) Absorption cross section of different oligomers excited with linearly polarized light and (b) Fourier spectrum of the field oscillations in the hot spots for different oligomers. (c) The electric field profile in the frequency domain from Lumerical FDTD simulations for the quadrumer, hexamer and decamer at 880 nm (the arrows show the direction of polarization of the excitation beam). (d-e) The electric field oscillation in a hot spot for various oligomers.

4. Oligomer based plasmonic nanolaser

We designed and simulated plasmon lasers based on the oligomers described above (dimer, quadrumer, hexamer, decamer, 18-mer) on top of a glass plate and surrounded by a gain medium (organic dye) (see Fig. 4(c)). Based on the simulation, most of the modes, for such gold oligomers, oscillate in the region above 1.24 eV (below 1000 nm). We choose one of the organic dyes as the gain medium with a photoluminescence peak between 620-1000 nm to match the plasmonic oscillations, namely IR-140 (5,5′-Dichloro-11-diphenylamino-3,3′-diethyl-10,12-ethylenethiatricarbocyanine perchlorate) with an absorption peak around 820 nm (linewidth around 100 nm) and a photoluminescence peak around 880 nm [33] (linewidth around 80 nm) in a solution of the dimethyl sulfoxide (DMSO) with molar concentrations 0.25-1 mM.

We use one of the localised surface plasmons of the nano oligomer, excited by incoming pump beam [34], to achieve a desirable population inversion between the ground and upper laser levels in the area of the excited plasmon oscillation. This will provide the required gain to reach the lasing condition of the selected mode, i.e. the total absorption and radiation losses during the mode oscillation is less than the total gain [20]. At the same time, the oscillation frequency of the oligomer lasing mode must fit the maximum of the PL spectrum of the gain medium to reach maximum lasing efficiency. Additionally, we have to match the pump mode and the lasing mode in the gain medium region (see Eq. (4)) to increase the pumping efficiency. In Fig. 3(c), we see the Lumerical simulation of the near electric field distribution for the dark modes of the quadrumer, hexamer and decamer, which must spatially match the pump beam (see Eq. (4)).

Optics EXPRESS

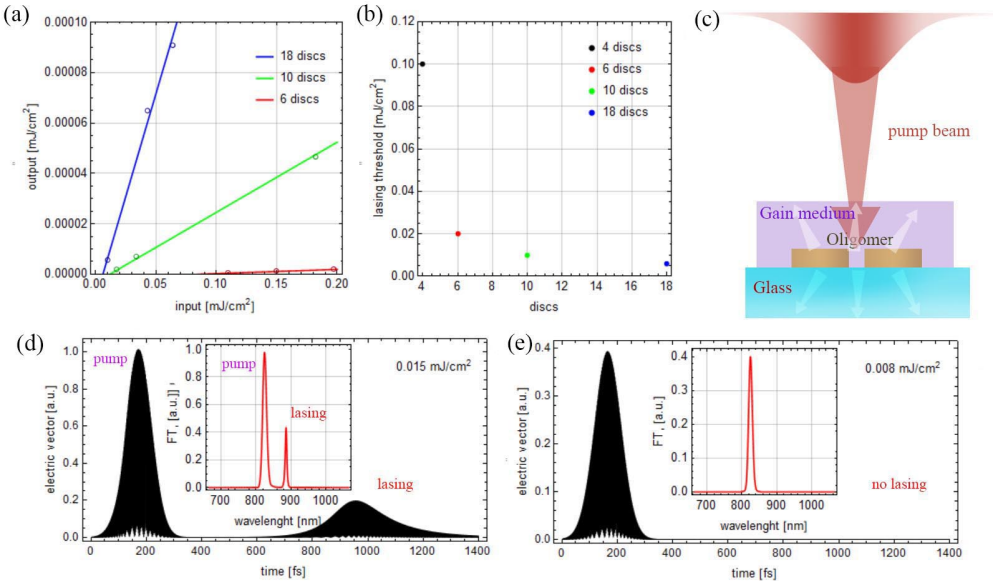

Fig. 4. (a) The slope efficiencies and (b) the lasing thresholds for the oligomer based plasmonic nano lasers. (c) The schematic of the plasmonic nanolaser and the pump beam. (d-e) The electric field oscillation in the hot spot for the decamer plasmonic nanolaser and the corresponding Fourier spectra.

Based on the investigation of the temporal and spectral behaviour of excited modes around IR-140 PL maximum (see section above), we see that increasing the complexity of the oligomer geometry (more gold discs combining the oligomer) increases the plasmon lifetime and narrows the absorption and Fourier spectra of the excited plasmons. This leads to an increase of the resonator quality factor [30] by a factor of three from the quadrumer to the decamer. Moreover, to increase the lifetime and decrease the linewidth of the oscillating plasmon we can use the oligomer modes with close to zero net dipole moment and longer lifetime (dark modes) as the lasing modes (see Fig. 2(c)). Furthermore, implementing a gain medium with a narrow PL linewidth improves lasing efficiency. The narrow linewidth, based on the uncertainty principle, increases the lifetime of the excited electron ($\Delta\omega \sim 1/\tau_{21}$) on the lasing level 2 (see Fig. 1) and can improve the lasing efficiency. Additionally, the use of a gain medium with a narrow PL linewidth can increase the lasing efficiency due to a narrow stimulated photon dispersion, which increases the probability of stimulated photons to be released [34].

In Fig. 4(d), (e) we see the electric vector oscillation and the corresponding Fourier spectra in the hot spot below (e) and above (d) the lasing threshold of a decamer–based plasmonic nanolaser, obtained by the FDTD (four-level two-electron) simulation. In the Fourier spectra, we see two main peaks: 820 nm (pump) and 880 nm (lasing). We have used a 100 fs laser pulse (with spectral peak around 820 nm and 9.8 nm spectral bandwidth) to pump the oligomer with a Gaussian intensity distribution of 1 μm beamwidth. A second 880 nm pulse develops after 1 ps of the pump pulse. It represents the lasing mode oscillation (~180 fs) with ~5 nm spectral bandwidth. The oligomer geometry and complexity determine the lasing threshold and lasing efficiency. The lasing thresholds and slope efficiencies differ significantly for the various oligomer designs (see Fig. 4(a), (b)). In the case of the longer lifetime lasing mode oscillation we were able to decrease the lasing threshold significantly. For our specific case of the oligomer design (100 nm diameter gold discs with 20 nm gaps), we have decreased the lasing threshold from the quadrumer to the 18-mer by a factor of ten, the respective SP lifetime tripled (see Fig. 4(b)). Additionally, we

Optics EXPRESS

see that the slope efficiency improved considerably as well (see Fig. 4(a)). We observe a linear behaviour of the slope efficiency in the simulation, however, including the thermal effect in the simulation can lead to a non-linear behaviour of the slope efficiency curve.

One reason for the improved lasing efficiency is the increase of the resonator quality factor due to the narrowing of the spectral linewidth (plasmon lifetime increase) of the oscillating lasing plasmon, which leads to an increase in the Purcell factor and LDOS. Moreover, the increase of the plasmon lifetime raises the probability of stimulated emission in the case of the plasmon lifetime much shorter than the laser upper level lifetime (<100 fs versus 1 ns in our case, for plasmon lifetime and IR-140 (DMSO) upper lasing level 2 lifetime respectively) (see Fig. 1) [33]. Finally, the increase of the lifetime of the excited pump plasmon increases the pumping time of the gain medium, therefore increasing the probability of the ground level 0 electron (see Fig. 1) to get excited.

An additional reason can be the number of hot spots and the intensity enhancement value in these hot spots of oscillating pump plasmon for the different oligomer designs. The number of gold discs composing the oligomer influences the number of hot spots appearing in the gaps between neighbouring discs. Besides, increasing the oligomer spatial size increases the amount

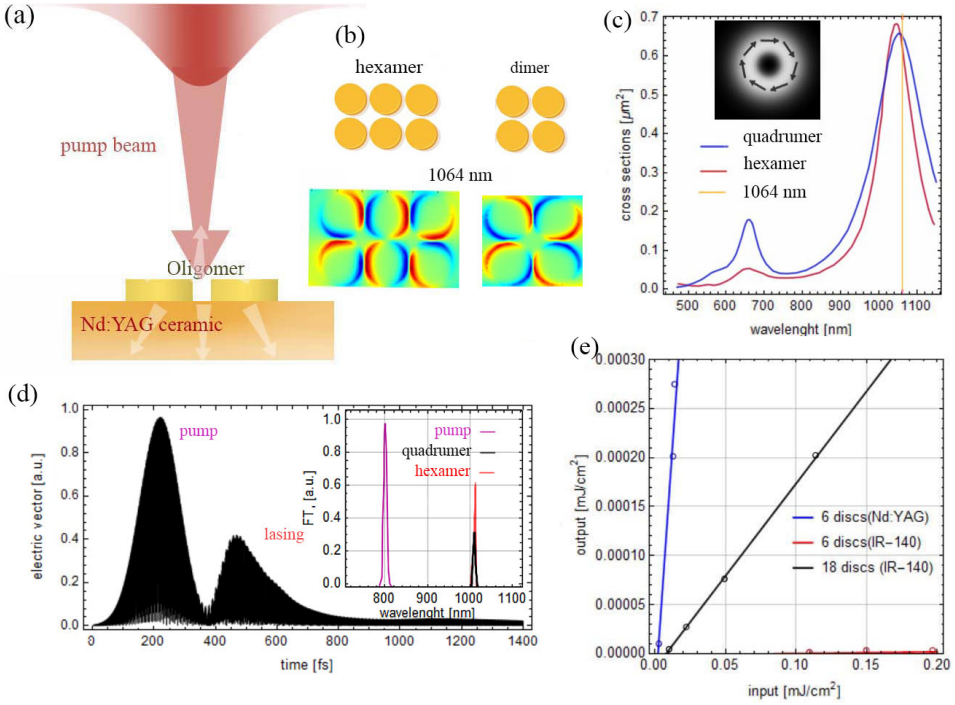

Fig. 5. (a) The schematic of the plasmonic nanolaser on Nd:YAG ceramic gain medium and the pump beam. (b) The gold nanodisk oligomers for Nd:YAG nanolaser with respective electric field profiles (A2g mode) at lasing wavelength. (c) The absorption cross section of hexamer and quadrumer on top of a dielectric material with a refractive index similar to Nd:YAG (n = 1.8) excited by azimuthally polarised light [20]. (d) The electric field oscillation in a hot spot for the Nd:YAG hexamer plasmonic nanolaser and the respective Fourier spectra (quadrumer Fourier spectra obtained with a pump pulse of similar energy). (e) Comparison of the slope efficiencies of hexamer based plasmonic nanolasers with Nd:YAG and IR-140 gain materials.

Optics EXPRESS

of the pump beam energy which is absorbed during the excitation of the pump plasmon, for the case of the oligomer size smaller than the beam width of the pump beam.

4.1. Nd^{3+}:YAG gain

We simulated a plasmonic nanolaser based on the gold hexamer on top of a Nd:YAG ceramic slab (see Fig. 5(a), (b)). The size of the hexamer discs diameter (150 nm) and geometry were adjusted to receive the plasmon oscillation maximum at the emission peak of the Nd^{3+}:YAG (1064 nm) (see Fig. 5(b)). A_{2g} (azimuthal) dark mode [20] at 1064 nm was selected as the lasing mode (see Fig. 5(b)). The pump beam at 808 nm is a linearly polarized Gaussian beam with $w_0 = 1$ μm (beam width), $\tau = 100$ fs (pulse duration) and $\Delta\lambda = 9.6$ nm (spectral linewidth). The gap between the oligomers was the same as for the IR-140 case described above, namely 20 nm. The resulting enhancement in the gap between the gold discs was close to IR-140. The main difference of the solid-state gain material from IR-140 organic dye is the narrowed absorption (808 nm) and emission (1064 nm) peaks, namely around 1-2 nm of linewidth only [35]. Compared to IR-140, the Nd^{3+}:YAG gain medium shows a decrease of the lasing threshold (around 10 times) and an improved slope efficiency (see Fig. 5(e)). Based on the simulation we see that the gain medium with such a narrow emission spectra linewidth plays a key role in the lasing process, and we were able to achieve the efficient lasing at such a low quality factor (~10) (see Fig. 5(d)). The emission spectra linewidth narrowing increases the lifetime of the excited electron in the lasing level 2 (see Fig. 1) and decreases the frequency difference of the stimulated photon, which results in the improvement of the lasing efficiency.

We see that, due to quite spectrally wide plasmon resonance in the nano oligomers (see Fig. 5(c)) it is favourable to use the gain medium with narrow emission peak (as an example the solid state gain material). In the case of the organic dye gain material, it is critically important to narrow the lasing plasmon oscillation linewidth. One way to do this is to increase the amount of nano discs composing the oligomer, which can significantly increase the plasmon laser efficiency and decrease the lasing threshold.

5. Conclusion

We have investigated the influence of the laser quality factor and the emission property of the gain medium in the oligomer based plasmonic nanolaser. We have shown that the oligomer geometry and complexity influence the lasing threshold and the lasing efficiency dramatically. The reason for such improvement of the lasing efficiency is the increase of the resonator quality factor due to the narrowing of the spectral linewidth and the extension of the lasing plasmon lifetime, which leads to an increase in the Purcell factor and LDOS. One of the ways of narrowing the spectral linewidth can be to increase the number of nano discs composing the oligomer, it can significantly increase the plasmon laser efficiency and decrease the lasing threshold. Additionally, we have shown that it is significantly advantageous to use the gain medium with narrow emission peak (as example solid state gain material) in the nano plasmonic lasers due to quite spectrally wide plasmon resonances in the nano oligomers.

Funding. Freie Universität Berlin; European Research Council (772108).

Disclosures. The authors declare that there are no conflicts of interest related to this article.

Data availability. Data underlying the results presented in this paper are not publicly available at this time but may be obtained from the authors upon reasonable request.

References

1. J. A. Schuller, E. S. Barnard, W. Cai, Y. C. Jun, J. S. White, and M. L. Brongersma, "Plasmonics for extreme light concentration and manipulation," Nat. Mater. **9**(3), 193–204 (2010).
2. D. K. Gramotnev and S. I. Bozhevolnyi, "Plasmonics beyond the diffraction limit," Nat. Photonics **4**(2), 83–91 (2010).
3. E. L. Ru and P. Etchegoin, *Principles of Surface-Enhanced Raman Spectroscopy: and Related Plasmonic Effects*, (Elsevier, 2008).

Optics EXPRESS

4. L. Mingzhao, T.-W. Lee, S. K. Gray, P. Guyot-Sionnest, and M. Pelton, "Excitation of dark plasmons in metal nanoparticles by a localized emitter," Phys. Rev. Lett. **102**(10), 107401 (2009).
5. K. Sakai, T. Yamamoto, and K. Sasaki, "Nanofocusing of structured light for quadrupolar light-matter interactions," Sci. Rep. **8**(1), 7746 (2018).
6. E. Prodan, C. Radloff, N. J. Halas, and P. Nordlander, "A Hybridization Model for the Plasmon Response of Complex Nanostructures," Science **302**(5644), 419–422 (2003).
7. N. S. Mueller, B. G. M. Vieira, F. Schulz, P. Kusch, V. Oddone, E. B. Barros, H. Lange, and S. Reich, "Dark interlayer plasmons in colloidal gold nanoparticle bi-and few-layers," ACS Photonics **5**(10), 3962–3969 (2018).
8. S. I. Azzam, A. V. Kildishev, R. M. Ma, C. Z. Ning, R. Oulton, V. M. Shalaev, M. I. Stockman, J. L. Xu, and X. Zhang, "Ten years of spasers and plasmonic nanolasers," Light: Sci. Appl. **9**(1), 90 (2020).
9. R. S. Savelev, A. P. Slobozhanyuk, A. E. Miroshnichenko, Y. S. Kivshar, and P. A. Belov, "Subwavelength waveguides composed of dielectric nanoparticles," Phys. Rev. B **89**(3), 035435 (2014).
10. R. F. Oulton, V. J. Sorger, T. Zentgraf, R. M. Ma, C. Gladden, L. Dai, G. Bartal, and X. Zhang, "Plasmon lasers at deep subwavelength scale," Nature **461**(7264), 629–632 (2009).
11. N. I. Zheludev, S. L. Prosvirnin, N. Papasimakis, and V. A. Fedotov, "Lasing Spaser," Nat. Photonics **2**(6), 351–354 (2008).
12. W. Zhou, M. Dridi, J. Y. Suh, C. H. Kim, D. T. Co, M. R. Wasielewski, G. C. Schatz, and T. W. Odom, "Lasing Action in Strongly Coupled Plasmonic Nanocavity Arrays," Nat. Nanotechnol. **8**(7), 506–511 (2013).
13. A. Yang, T. B. Hoang, M. Dridi, C. Deeb, M. H. Mikkelsen, G. C. Schatz, and T. W. Odom, "Real-Time Tunable Lasing from Plasmonic Nanocavity Arrays," Nat. Commun. **6**(1), 6939 (2015).
14. M. Ramezani, A. Halpin, A. I. Fernández-Domínguez, J. Feist, S. R.-K. Rodriguez, F. J. Garcia-Vidal, and J. Gomez Rivas, "Plasmon-Exciton-Polariton Lasing," Optica **4**(1), 31 (2017).
15. P. Molina, E. Yraola, M. O. Ramírez, C. Tserkezis, J. L. Plaza, J. Aizpurua, J. Bravo-Abad, and L. E. Bausá, "Plasmon-assisted Nd3+-based solid-state nanolaser," Nano Lett. **16**(2), 895–899 (2016).
16. Y. L. Ho, J.K. Clark, A.S.A. Kamal, and J. J. Delaunay, "On-chip monolithically fabricated plasmonic-waveguide nanolaser," Nano Lett. **18**(12), 7769–7776 (2018).
17. J. B. Herzog, M. W. Knight, Y. Li, K. M. Evans, N. J. Halas, and D. Natelson, "Dark plasmons in hot spot generation and polarization in interelectrode nanoscale junctions," Nano Lett. **13**(3), 1359–1364 (2013).
18. R. Yang, C. Dai, C. Wan, G. Zheng, and Z. Li, "Planar ultrathin omni-directional perfect absorber utilizing amorphous silicon for photovoltaics," Opt. Mater. Express **10**(2), 532–539 (2020).
19. A. Amina, F. Arduini, D. Moscone, G. Palleschi, and V. Scognamiglio, "Nanostructured (Bio) sensors for smart agriculture," TrAC, Trends Anal. Chem. **98**, 95–103 (2018).
20. I. A Litvin, N. S Mueller, and S. Reich, "Selective excitation of localized surface plasmons by structured light," Opt. Express **28**(16), 24262–24274 (2020).
21. D. Wang, W. Wang, M. P. Knudson, G. C. Schatz, and T. W. Odom, "Structural engineering in plasmon nanolasers," Chem. Rev. **118**(6), 2865–2881 (2018).
22. S. H. Chang and A. Taflove, "Finite-difference time-domain model of lasing action in a four-level two-electron atomic system," Opt. Express **12**(16), 3827–3833 (2004).
23. U. Hohenester and J. Krenn, "Surface plasmon resonances of single and coupled metallic nanoparticles: A boundary integral method approach," Phys. Rev. B **72**(19), 195429 (2005).
24. J.D. Jackson, *Classical electrodynamics* (John Wiley & Sons, Ltd., 1999).
25. I. A. Litvin, "Implementation of intra-cavity beam shaping technique to enhance pump efficiency," J. Mod. Opt. **59**(3), 241–244 (2012).
26. D. Naidoo, I. A. Litvin, and A. Forbes, "Brightness enhancement in a solid-state laser by mode transformation," Optica **5**(7), 836–843 (2018).
27. L. Novotny and B. Hecht, *Principles of Nano-Optics* (Cambridge Univ. Press, 2006).
28. E. M. Purcell, "Spontaneous emission probabilities at radio frequencies," Phys. Rev. **69**(1-2), 37–38 (1946).
29. H. Altug, D. Englund, and J. Vuckovic, "Ultrafast photonic crystal nanocavity laser," Nat. Phys. **2**(7), 484–488 (2006).
30. W. Zhou, Y. Hua, M. D. Huntington, and T. W. Odom, "Delocalized lattice plasmon resonances show dispersive quality factors," J. Phys. Chem. Lett. **3**(10), 1381–1385 (2012).
31. E. Le Ru and P. Etchegoin, *Principles of surface enhanced Raman spectroscopy: and related plasmonic effects*, (Elsevier Science, New York, 2008).
32. V. Deinhart, L. M. Kern, J. N. Kirchhof, S. Juergensen, J. Sturm, E. Krauss, T. Feichtner, S. Kovalchuk, M. Schneider, D. Engel, and B. Pfau, "The patterning toolbox FIB-o-mat: Exploiting the full potential of focused helium ions for nanofabrication," Beilstein J. Nanotechnol. **12**(1), 304–318 (2021).
33. J. P. Fouassier, D. J. Lougnot, and J. Faure, "Photoisomerization processes in the IR-140 laser dye," Opt. Commun. **23**(3), 393–397 (1977).
34. A. E. Siegman, *Lasers* (University Science, Mill Valley, Calif., 1986).
35. J. E. Geusic, H. M. Marcos, and L. Van Uitert, "Laser oscillations in Nd-doped yttrium aluminum, yttrium gallium and gadolinium garnets," Appl. Phys. Lett. **4**(10), 182–184 (1964).